REVIEW SUMMARY

THERMOELECTRICS

Advances in thermoelectric materials research: Looking back and moving forward

Jian He* **and Terry M. Tritt***

BACKGROUND: Heat and electricity are two forms of energy that are at opposite ends of a spectrum. Heat is ubiquitous, but with low quality, whereas electricity is versatile, but its production is demanding. Thermoelectrics offers a simple and environmentally friendly solution for direct heat-to-electricity conversion. A thermoelectric (TE) device can directly convert heat emanating from the Sun, radioisotopes, automobiles, industrial sectors, or even the human body to electricity. Electricity also can drive a TE device to work as a solid-state heat pump for distributed spot-size refrigeration. TE devices are free of moving parts and feasible for miniaturization, run quietly, and do not emit greenhouse gasses. The full potential of TE devices may be unleashed by working in tandem with other energy-conversion technologies.

Thermoelectrics found niche applications in the 20th century, especially where efficiency was of a lower priority than energy availability and reliability. Broader (beyond niche) application of thermoelectrics in the 21st century requires developing higher-performance materials. The figure of merit, *ZT*, is the primary measure of material performance. Enhancing the *ZT* requires optimizing the adversely interdependent electrical resistivity, Seebeck coefficient, and thermal conductivity, as a group. On the microscopic level, high material performance stems from a delicate concert among tradeoffs between phase stability and instability, structural order and disorder, bond covalency and ionicity, band convergence and splitting, itinerant and localized electronic states, and carrier mobility and effective mass.

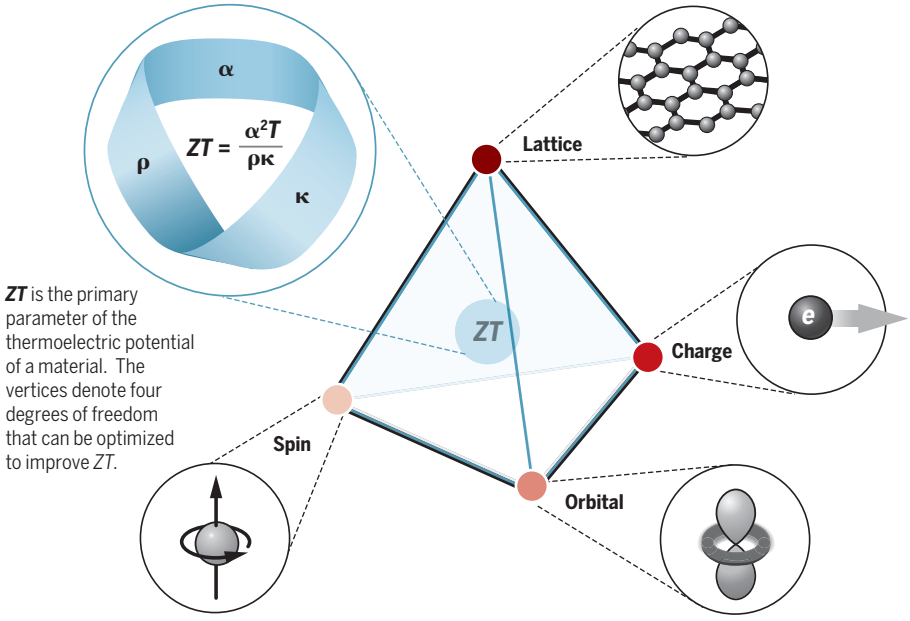

ZT is the primary parameter of the thermoelectric potential of a material. The vertices denote four degrees of freedom that can be optimized to improve *ZT*.

GRAPHIC: ADAPTED BY K. SUTLIFF/*SCIENCE*

Thermoelectric materials research is an application-driven multidisciplinary topic of fundamental research, which involves the charge, spin, orbital, and lattice degrees of freedom of material. The electrical resistivity (σ), Seebeck coefficient (α), and thermal conductivity (κ) are optimized as a group via synergistic synthesis-experimental-theoretical efforts toward a high figure of merit *ZT* and, thus, high-efficiency thermoelectric devices.

ADVANCES: Innovative transport mechanisms are the fountain of youth of TE materials research. In the past two decades, many potentially paradigm-changing mechanisms were identified, e.g., resonant levels, modulation doping, band convergence, classical and quantum size effects, anharmonicity, the Rashba effect, the spin Seebeck effect, and topological states. These mechanisms embody the current states of understanding and manipulating the interplay among the charge, lattice, orbital, and spin degrees of freedom in TE materials. Many strategies were successfully implemented in a wide range of materials, e.g., V_2VI_3 compounds, VVI compounds, filled skutterudites and clathrates, half-Heusler alloys, diamond-like structured compounds, Zintl phases, oxides and mixed-anion oxides, silicides, transition metal chalcogenides, and organic materials. In addition, advanced material synthesis and processing techniques, for example, melt spinning, self-sustaining heating synthesis, and field-assisted sintering, helped reach a much broader phase space where traditional metallurgy and melt-growth recipes fell short. Given the ubiquity of heat and the modular aspects of TE devices, these advances ensure that thermoelectrics plays an important role as part of a solutions package to address our global energy needs.

ON OUR WEBSITE

Read the full article at http://dx.doi.org/10.1126/science.aak9997

OUTLOOK: The emerging roles of spin and orbital states, new breakthroughs in multiscale defect engineering, and controlled anharmonicity may hold the key to developing next generation TE materials. To accelerate exploring the broad phase space of higher multinary compounds, we need a synergy of theory, machine learning, three-dimensional printing, and fast experimental characterizations. We expect this synergy to help refine current materials selection and make TE materials research more data driven. We also expect increasing efforts to develop high-performance materials out of nontoxic and earth-abundant elements. The desire to move away from Freon and other refrigerant-based cooling should shift TE materials research from power generation to solid-state refrigeration. International round-robin measurements to cross-check the high *ZT* values of emerging materials will help identify those that hold the most promise. We hope the renewable energy landscape will be reshaped if the recent trend of progress continues into the foreseeable future. ■

Department of Physics and Astronomy, Clemson University, Clemson, SC 29634-0978, USA.
*Corresponding author. Email: jianhe@g.clemson.edu (J.H.); ttritt@clemson.edu (T.M.T.)
Cite this article as J. He, T. M. Tritt, *Science* **357**, eaak9997 (2017). DOI: 10.1126/science.aak9997

REVIEW

THERMOELECTRICS

Advances in thermoelectric materials research: Looking back and moving forward

Jian He* and Terry M. Tritt*

High-performance thermoelectric materials lie at the heart of thermoelectrics, the simplest technology applicable to direct thermal-to-electrical energy conversion. In its recent 60-year history, the field of thermoelectric materials research has stalled several times, but each time it was rejuvenated by new paradigms. This article reviews several potentially paradigm-changing mechanisms enabled by defects, size effects, critical phenomena, anharmonicity, and the spin degree of freedom. These mechanisms decouple the otherwise adversely interdependent physical quantities toward higher material performance. We also briefly discuss a number of promising materials, advanced material synthesis and preparation techniques, and new opportunities. The renewable energy landscape will be reshaped if the current trend in thermoelectric materials research is sustained into the foreseeable future.

The world has been keeping up with an ever-increasing demand of electricity by burning more and more fossil fuels since the second Industrial Revolution. However, fossil fuels are not renewable: The world's crucial reliance on fossil fuels and the environmental concerns of burning fossil fuels are putting both human and natural systems at stake. On the other hand, heat can be considered renewable in that it is ubiquitous and inevitable: Thermal processes generate >90% of the energy we use, whereas the energy we waste is primarily and ultimately in the form of heat (*1*). Thermoelectrics is the simplest technology applicable to direct heat-to-electricity energy conversion (*2*–*4*).

On the basis of the Seebeck, Peltier, and Thomson effects discovered in the 19th century, thermoelectrics has found niche applications in the 20th century, especially "where cost and efficiency were not as important as energy availability, reliability, and predictability" (*5*). A thermoelectric (TE) device is all solid state; free of moving parts, noises, or greenhouse emissions; and feasible for miniaturization, making it ready to work in tandem with other energy-conversion technologies (*6*). It is also a prime choice in distributed spot-size active heat management (*7*). The examples range from μW- to mW-level wristwatch and pacemaker batteries, 10- to 100-W-level radioisotope TE power generators (RTGs) for NASA's deep-space probes, 10- to 100-W-level microelectronics and wine coolers, 100-W-level car seat climate-control systems to kW-level waste-heat harvesting for automobiles (*8*). In the 2015 20th Century Fox movie *The Martian*, it was the NASA RTG that allowed astronaut Mark Watney to survive for many months stranded on Mars.

Currently, the efficiency of thermoelectrics is lower than other energy-conversion technologies because of the low performance of TE material (Fig. 1) (*9*). Broader (beyond niche) application of thermoelectrics further into the 21st century is thus hinged on developing higher-performance materials. Over two decades ago, one of the authors of this paper wrote a *Science* Perspective (*10*) related to one of the exciting new TE materials at that time, filled skutterudites (*11*). Since then, we have witnessed many strides in material performance (Fig. 2) and thus a continually improved status of thermoelectrics (Fig. 1). The renewable energy landscape could very well be reshaped if the current trend in TE materials research is sustained into the foreseeable future.

Material performance

The TE promise of a material is measured by three combinatorial material parameters. The primary parameter is the dimensionless figure of merit, *ZT*, which helps us determine the "efficiency." The maximum power-generation efficiency of a TE material, η, is

$$\eta = \left(\frac{T_{hot} - T_{cold}}{T_{hot}}\right)\left[\frac{\sqrt{1+ZT_m}-1}{\sqrt{1+ZT_m}+\left(\frac{T_{cold}}{T_{hot}}\right)}\right] \quad (1)$$

where the Carnot efficiency is the ratio of the temperature difference between the hot end and the cold end ($T_{hot} - T_{cold}$) to T_{hot}. The coefficient of performance for TE refrigeration adopts a slightly different expression, but in the same spirit (*2*). The definition of *ZT* is

$$ZT = \frac{\alpha^2 T}{\rho\kappa} = \frac{\alpha^2 T}{\rho(\kappa_L + \kappa_e)} = \frac{PF}{\kappa} \quad (2)$$

where α is the Seebeck coefficient (i.e., the thermopower), ρ is the electrical resistivity, κ is the thermal conductivity, *PF* is the power factor, *T* is the temperature in kelvin, κ_L is the lattice (phonon and magnon) thermal conductivity, and κ_e is the charge-carrier thermal conductivity. The α value is positive for p-type (hole) conduction and negative for n-type (electron) conduction. Through Eqs. 1 and 2, the grand problem of TE energy conversion is shifted to optimizing three macroscopically measurable transport parameters (ρ, α, and κ) as a group. As shown in Fig. 2, most state-of-the-art TE materials have their maximum *ZT* values between 1 and 2.5 due to the adversely interdependent (ρ, α, and κ). Note that the ZT_m in Eq. 1 is the average *ZT* value between T_{cold} and T_{hot}, whereas the *T* in Eq. 2 refers to a specific temperature. A large ZT_m value over a wide temperature range is more practical than a *ZT* spike in applications. From an efficiency standpoint, a ZT_m value ~3 to 4 is needed for thermoelectrics to compete with other energy-generation technologies.

The second combinatory material parameter is the TE quality factor (i.e., the *B* factor) (*2*, *12*, *13*). The *B* factor is derived from Eq. 2 but defined with microscopic band structure and transport parameters (*14*). For a one-band nondegenerate semiconductor

$$B \propto \frac{\mu_c m^{*1.5} T^{2.5}}{\kappa_L} \quad (3)$$

where m^* is the effective mass and μ_c is the carrier mobility at the nondegenerate (classical) limit. For a given scattering mechanism and at any Fermi energy E_F, the higher the *B* value, the higher the *ZT* value. The *B* factor showcases the importance of decoupling the electrical conductivity–governing μ_c and the Seebeck coefficient–governing m^* while minimizing the κ_L. In practice, Eq. 3 remains a useful indicator for prescreening and optimizing more-complex materials (*14*). The third combinatorial material parameter is the TE compatibility factor *S* (*15*)

$$S = \frac{\sqrt{1+ZT}-1}{\alpha T} \quad (4)$$

The *S* is a device-design parameter, defined by the macroscopic measurable parameters (ρ, α, and κ). It rationalizes how to extract the maximum efficiency out of a material by optimizing its geometrical shape, compositional gradient, or segmentation of a TE-device leg with different materials. For completeness, it is recommended that all three combinatorial material parameters (*ZT*, *B*, and *S*) are assessed in the TE study of a material.

General aspects of the TE process

Although each TE material is specific, the TE process embodied in the material can be generalized in the context of linear nonequilibrium thermodynamics of coupled dissipative processes (*16*). A TE process is no more than a heat engine using electrons and holes as the working medium. The

Department of Physics and Astronomy, Clemson University, Clemson, SC 29634-0978, USA.
*Corresponding author. Email: jianhe@g.clemson.edu (J.H.); ttritt@clemson.edu (T.M.T.)

magnitude of α and the *ZT* of a material are rooted in the entropy and entropy production of the TE process therein, respectively.

The magnitude of the Seebeck coefficient measures the average entropy carried by a charge carrier divided by its charge in the limit of thermal equilibrium (*17*). To help illustrate the relation between the Seebeck coefficient and the microscopic band structure and transport parameters, we present an approximate formula derived from the Bethe-Sommerfeld expansion of the Mott relation for degenerate statistics and single-band conduction (*18*)

$$\alpha = \frac{\pi^2}{3}\frac{k_B^2 T}{e}\left[\frac{\mathrm{DOS}(E)}{n(E)} + \frac{1}{\mu(E)}\frac{d\mu(E)}{dE}\right]\Bigg|_{E=E_F} \quad (5)$$

where e is the carrier charge, DOS(E) is the energy-dependent electronic density of states, $n(E)$ is the energy-dependent number of states, k_B is the Boltzmann constant, and μ is the energy-dependent carrier mobility. Despite a limited applicability, Eq. 5 clearly shows that the larger the DOS(E_F), the stronger the energy dependence of μ, and the higher the $|\alpha|$. These arguments hold in more-complex materials and act as the guideline for band structure and transport engineering.

The *ZT* value of a material reflects how reversible the TE process is in the material (*16*). In the case of zero entropy production, the TE process is reversible, the *ZT* of the material →∞, and the Carnot efficiency is reached (*19*). The Carnot efficiency is the upper efficiency limit of a TE process cycle, as with any heat-engine cycle. The entropy production in a TE process is the fundamental cause of irreversibility. The irreversible factor, derived from the compatibility factor *S*, gauges the sensitivity of the efficiency to the working condition. Generally, the higher the *ZT* value, the higher the sensitivity to the variation of working conditions (*16*). Enhancing the *ZT* of a material is thus tied to minimizing the entropy production of the TE process therein. According to Callen (*20*), the entropy production in a TE process arises from the heat flow from the hot end to the cold end and also from the degradation of electrochemical potential into heat (i.e., the dissipation effect, such as Joule heating).

Recent advances in TE materials research

Innovative transport mechanisms are the fountain of youth of TE materials research. This article reviews several potentially paradigm-shifting mechanisms enabled by defects, size effects, critical phenomena, anharmonicity, and the spin degree of freedom. These mechanisms embody the latest state of understanding and manipulating the interplay among charge, lattice, orbital, and spin degrees of freedom in TE materials. We use these mechanisms to guide the discussion of materials. Because of page limitations, the coverage of promising materials or synthesis and preparation techniques is purposely limited. The interested reader is referred to outstanding reviews on bulk (*4*, *21*) and nanostructured materials (*8*, *9*, *22*, *23*), materials chemistry (*24*, *25*), fundamentals of thermoelectricity (*9*, *26*–*28*), heat conduction (*29*, *30*), electrical transport (*31*), theoretical studies (*26*, *32*, *33*), and TE devices (*26*, *34*) for further reading.

Defect-enabled mechanisms

Defects arise from the breaking of translational and/or rotational symmetry of the crystal lattice. Defect engineering aims to tackle two or more otherwise adversely interdependent band structure and transport properties toward higher material performance. For instance, doping a semiconductor optimizes the carrier concentration to enhance the *PF* while the resulting point defects scatter heat-carrying phonons to suppress the κ_L (*2*). Defects can also activate the otherwise hibernating degree of freedom (*35*). The following subsections cover six defect-enabled mechanisms in the order of point defects (intrinsic point defects, resonant levels, band convergence), linear defects (dislocations), planar defects (interfacial preferential scattering), and bulk defects (modulation doping).

Intrinsic point defects

Identifying the correct causal chain is crucial in defect engineering, otherwise one risks getting the right result for the wrong reason. Taking the

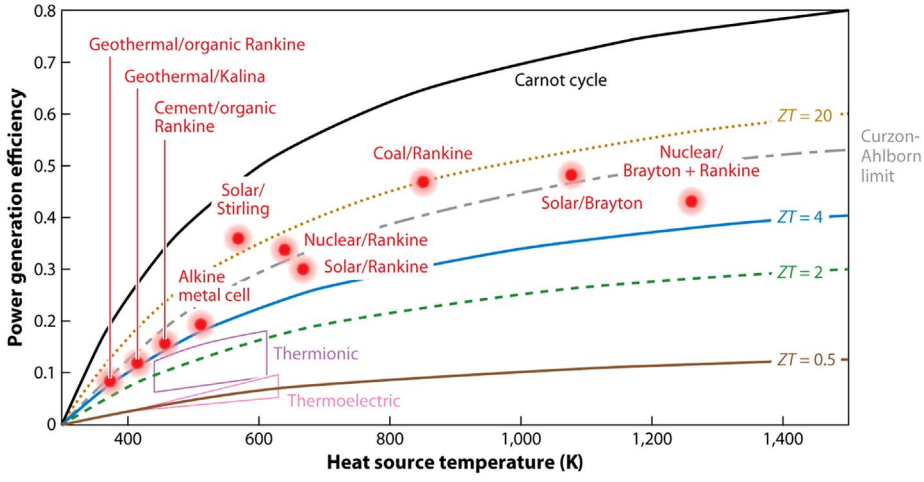

Fig. 1. Thermoelectrics in the global landscape of energy conversion. The efficiency comparison of thermoelectrics and other energy-conversion technologies as a function of the heat-source temperature. The *ZT* values are assumed to be temperature independent, and the heat-sink temperature is set at room temperature. [Figure adapted from (*9*)]

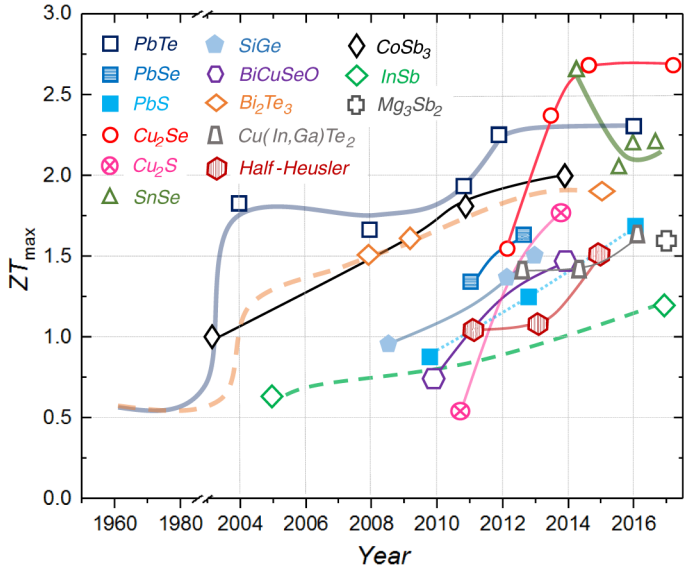

Fig. 2. Timeline of the maximum *ZT* values for several representative families of TE materials. PbTe (*129*, *38*, *130*, *50*, *131*), PbSe (*132*, *133*), PbS (*134*, *135*, *61*); Cu2Se (*110*, *67*, *136*, *112*), Cu2S (*137*, *138*); SnSe (*97*, *100*–*102*), Mg3Sb2 (*139*), SiGe (*140*–*142*), BiCuSeO (*143*, *144*), Bi2Te3 (*58*, *122*, *49*), Cu(In,Ga)Te2 (*145*, *45*, *146*), CoSb3 (*11*, *147*, *148*), InSb (*149*, *150*), and half-Heusler compounds (*151*, *152*, *107*).

benchmark material Bi_2Te_3 as an example, doping Sb on the Bi site and Se on the Te site led to high p-type and n-type performance, respectively. The dopants (extrinsic point defects) first facilitate the formation of intrinsic point defects (antisites, interstitials, and vacancies), and then the intrinsic point defects directly determine the carrier concentration, thereby enhancing the material performance. Zhu *et al.* reviewed the role of intrinsic point defects in V_2VI_3 compounds and showed that intrinsic point defects could be manipulated compositionally, mechanically, and thermally (*36*). In particular, the electronegativity difference and the covalent radius difference between the cation and the anion effectively regulate the formation of cation antisites and anion vacancies. Intrinsic point defects are ubiquitous; a better understanding of intrinsic point defects and the interplay with other types of defects will enable more innovative defect engineering efforts.

Resonant levels

Resonant levels (RLs) refer to the impurity levels that lie in the conduction or valence band of the host material. Considering Eq. 5 and the Drude model $\sigma = ne\mu = ne^2\tau/m^*$, a large DOS($E_F$) and a strong energy dependence of relaxation time τ enhance the $|\alpha|$. Accordingly, the role of the RLs scheme is dual (*37*): (i) RLs induce a DOS peak that centers at the resonant energy E_D and (ii) RLs conduct and resonantly scatter charge carriers and the resonant scattering relaxation time often adopts a Lorentzian line shape $\tau_r(E) = \tau_0\left[1+\left(\frac{E-E_D}{\Gamma/2}\right)\right]^2$, where Γ is the energy range over which the phase-angle shift changes from 0 to π. A $|\alpha|$ significantly higher than what a Pisarenko plot predicts suggests the presence of RLs, but it takes the Nernst effect, magneto-Seebeck measurements, and theoretical calculations to confirm their presence (*38*). The efficacy of RLs is subject to properly positioning the E_D relative to the E_F and the Γ value; the s and p states (orbitals) of impurity are more practical than the 3d and f states in the RLs scheme (*37*).

Band convergence

Doping to actively align the electron bands for a higher degree of band degeneracy lies at the heart of the band-convergence scheme. The aim is to enhance the $|\alpha|$ without substantially degrading the σ. The band degeneracy has two contributors: (i) Multiple bands have their band energy extrema within a few k_BT of the E_F (i.e., the orbital degeneracy) and (ii) the Fermi surface has multiple carrier pockets due to crystal symmetry (i.e., the valley degeneracy). The valley degeneracy, N_v, factors into the DOS effective mass as $N_v^{2/3}$ (*39*). The Snyder group at Caltech implemented the band-convergence scheme in PbTe (*40*–*42*) and $CoSb_3$ (*43*). A similar scheme was successfully implemented in Mg_2(Sn,Si) (*44*), chalcopyrites (*45*), and Te-Ag-Ge-Sb (TAGS) (*46*). In particular, Zhang *et al.* devised a "pseudocubic approach" to attain a complex architecture that contains a long-range cubic framework coexisting with short-range noncubic lattice distortions (Fig. 3), giving rise to the high band convergence required for a high *PF* in less symmetric tetragonal chalcopyrites (*45*). The pseudocubic approach holds promise, however, for those low-symmetry materials that have an ideal band gap and a low κ_L. The band-convergence scheme and resonant-levels scheme worked jointly in attaining a $ZT \sim 1.4$ in SnTe via In and Cd codoping and nanostructuring (*47*). The efficacy of the band-convergence scheme is restricted by the temperature-induced band shift, interband scattering, and the solubility of dopants.

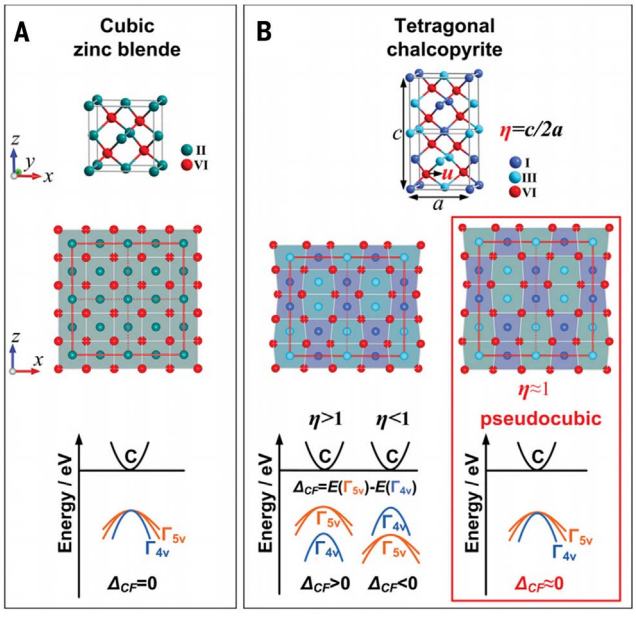

Fig. 3. The pseudocubic band-convergence scheme. (**A**) Crystal structure and schematic electron-band structure of cubic zinc blende structure. (**B**) Crystal structure and schematic electronic bands of ternary chalcopyrites. The *c* and *a* are the lattice constants along the *c*- and *a*-axis, respectively. Γ_{4v} is a nondegenerate band, and Γ_{5v} is a doubly degenerate band. Δ_{CF} is the crystal field–induced energy split at the top of the Γ_{4v} and Γ_{5v} bands. The pseudocubic structure has a cubic cation framework with $\Delta_{CF} \approx 0$ embedded in noncubic distorted anion framework. [Figure adapted from (*45*)]

Topological defects

Dislocations are one-dimensional (1D) defects; they are topological defects in that a dislocation cannot be fixed by any local rearrangement (*48*). Plastic deformation processes such as hot forging and extrusions are known to facilitate the formation of dislocations. Kim *et al.* used liquid flow–assisted sintering to synthesize p-type Bi_2Te_3 with dense dislocation arrays on low-energy grain boundaries (*49*). These dense dislocation arrays and the point defects within each grain strongly scattered heat-carrying phonons over a wide wavelength range, leading to very low κ_L values and, thus, state-of-the-art *ZT* values. The formation mechanism of dense dislocation arrays and the kinetics of dislocations under a temperature gradient are well worth further study.

Interfacial preferential scattering

Interfaces and grain boundaries are 2D planar defects. Ideally, an interface should render a three-tier preferential scattering: (i) scattering phonons more effectively than charge carriers, (ii) scattering low-energy charge carriers more effectively than high-energy charge carriers, and (iii) scattering minority charge carriers more effectively than majority charge carriers. Generally, coherent or semicoherent grain boundaries (*50*–*52*) and a proper intergrain band alignment (*52*, *53*) tend to retain the μ, whereas rough grain boundaries effectively suppress the κ_L (*54*, *55*). Interfaces and grain boundaries are convenient places to implement the carrier-energy filtering (CEF) scheme (*9*, *56*). The CEF scheme utilizes an energetic barrier to filter out the low-energy charge carriers to attain a higher $|\alpha|$. Note that the CEF effect and band alignment work to the opposite ends, so they must be properly balanced toward a high *PF*. In nanostructured Bi_2Te_3, it was inferred that the interfacial charged defects preferentially scattered the minority carriers more effectively than the majority carriers (*57*, *58*).

Modulation doping

Point defects tune the carrier concentration as effectively as they scatter the charge carriers and degrade the mobility. For nonresonant scattering, $\tau(E) \propto E^r$ (*59*), where r is the scattering parameter. We have r = 3/2 and r = 0 for ionized impurity scattering and charge-neutral impurity scattering, respectively. To mitigate this dilemma, "modulation doping" was devised for 2D structures by means of separating the charge carriers from the zonal dopants by spacer layers. The charge carriers donated from zonal dopants flow irreversibly into the high-mobility host matrix (i.e., the conduction channel); the mobility is thus retained. The modulation doping scheme is effective at temperatures where the ionized impurity scattering would otherwise predominate. Zebarjadi *et al.* modulation doped 3D $Si_{80}Ge_{20}$ host matrix with embedded $Si_{100}B_5$ nanoparticles without spacer layers (*60*). In self-assembled colloidal nanocrystals of PbS and Ag, Ag nanocrystals acted as the zonal dopants and phonon scatters and facilitated the band alignment among PbS nanograins, leading to a $ZT \sim 1.7$ at $T = 800$ K (*61*).

The "invisible dopants" scheme (*62*) is tied to the modulation doping scheme. The invisible dopants scheme is an "antiresonant" scattering in that the phase-angle shift is minimized by properly designing the potential profile of a core-shell nanoparticle. The scattering cross section of carrier–core shell nanoparticle exhibits a sharp dip within

a narrow energy range (i.e., the "cloaking window"), making the nanoparticle "invisible" to conduction electrons if the E_F is located within that energy range. The rapidly varying scattering cross section with energy near the E_F is also favored for a high $|\alpha|$. The efficacy of the modulation doping scheme is restricted by the element diffusion at high temperatures for a long period of time.

Size effects (reduced dimensionality)

Size effects underlie the paradigm of TE nanocomposites and low-dimensional TE materials (*8*, *22*, *23*). The classical and quantum size effects concern the scattering-limited mean free path and the confinement-induced change in the dispersion relation, respectively. For example, heat is carried by phonons with a wide, temperature-dependent spectrum of energy and momentum; suppressing the κ_L by limiting the phonon mean free path over a wide temperature range thus requires all-scale hierarchical microstructures (*50*). In the context of classical size effect, the κ_L has a minimum, i.e., the amorphous limit, when the phonon mean free path gets as small as the interatomic spacing and heat is carried by random-walking Einstein modes. The minimum lattice thermal conductivity κ_{min} is expressed as (*63*)

$$\kappa_{min} = \left(\frac{\pi}{6}\right)^{1/3} k_B n_a^{2/3} \sum_i v_i \left(\frac{T}{\theta_i}\right)^2 \int_0^{\theta_i/T} \frac{x^3 e^x}{(e^x-1)^2}\, dx \quad (6)$$

where the cutoff frequency is $\theta_i = v_i(\hbar/k_B)(6\pi^2 n_a)^{1/3}$, n_a is the number density of atoms, $\hbar$ is the reduced Planck's constant (Planck's constant h divided by 2π), and v_i is the sound velocity for each polarization mode.

The quantum size effect of charge carriers is used to create sharp electronic DOS features (*64*, *65*), favored for a high $|\alpha|$ upon properly positioning the E_F. When the de Broglie wavelength of charge carrier λ_d is comparable to the physical size of a material in one or more directions, the charge carriers are strongly confined in those directions and their dimensionality is thus reduced. Though differentiating the classical and quantum size effects is hard when they coexist, most of the advances in TE nanocomposites come from the interfacial scattering of heat-carrying phonons rather than from an enhanced DOS, suggesting that the classical size effect dominates the quantum size effect.

Critical phenomena-induced effects

According to Vining (*66*), the role of $(1 + ZT)$ in a TE process is equivalent to that of the ratio $\gamma_{Ei} = C_p/C_v$ in a gas-cycle engine, where C_p is the heat capacity at constant pressure and C_v is the heat capacity at constant volume. As shown in Fig. 4 (*9*), the γ_{Ei} diverges at a gas-liquid phase transition. It is plausible to argue that the ZT is enhanced near an electronic phase transition, as electrons are the working medium of a TE process. A ZT peak at the superionic phase transition of I-doped Cu_2Se was reported and attributed to the critical scattering of charge and heat carriers (*67*). The coupling of a continuous phase transition to charge-carrier transport led to an enhanced α and ZT in Ag-doped Cu_2Se (*68*). In these works, the critical fluctuations associated with the structural phase transition enable the charge carriers to access more microstates, thereby enhancing the $|\alpha|$. The use of structural entropy for enhancing the $|\alpha|$ near a critical point is restricted in practice because structural phase transitions are undesirable for TE devices. Hence, a great opportunity lies in the "subcritical" materials with an inherent electronic instability but no structural phase transition.

Anharmonicity

Although both aim to reduce the κ_L, scattering processes limit the phonon mean free path in the space domain, whereas anharmonicity limits the phonon lifetime in the time domain. Anharmonicity elicits intrinsically low κ_L via phonon-phonon interactions (*69*). In the caged compounds such as skutterudites and clathrates, the guest atom in the cage often rattles with a large anharmonic displacement at a low frequency; the interactions between the acoustic phonons and low-lying optical phonons are the key ingredient of the low κ_L values (*32*). Thermal expansion and the Grüneisen parameter γ are the macroscopic and microscopic measure of anharmonicity, respectively. Large complex unit cells with weak or asymmetric chemical bonding and heavy elements tend to have strong anharmonicity. At high temperatures, where the Umklapp process dominates, we have a simple, yet illustrative, formula (*70*)

$$\kappa_L = \frac{MV^{1/3}\theta_D^3}{\gamma^2 T} \quad (7)$$

where M, V, θ_D, and γ are average atomic mass, average atomic volume, the Debye temperature, and the volume (mode averaged) Grüneisen parameter, respectively. Most solids exhibit a γ value between 1 and 2, but a mode-specific Grüneisen parameter can be exceptionally large.

Several recent investigations are paving a way toward engineering anharmonicity. A resonant-bonding scenario was proposed to account for the low κ_L of IV-VI, V_2-VI_3, and V materials (*71*). In some phase-change materials, the amorphous state was found to be more harmonic than its crystalline counterpart, where resonant bonding acted as an amplifier of anharmonicity (*72*). Anharmonicity was believed to be fairly immune from structural imperfections because anharmonicity is rooted in the nature of chemical bonds (i.e., the entire occupied valence band), whereas impurities mostly act locally and affect the valence band edge. So, can we actively control anharmonicity? Jin *et al.* tuned the anharmonicity in InSb by a magnetic field (*73*). Actively controlling anharmonicity is a grand challenge, but also a great opportunity, in future TE material research.

Thermoelectrics needs a "spin"

The nomenclature "thermoelectric" may have left people with a wrong impression that thermoelectricity only involves the charge and lattice degrees of freedom. Indeed, the orbital degree of freedom of the dopant is crucial in the resonant-levels scheme. In addition, the spin entropy of charge carriers is a likely source of the large $|\alpha|$ of $Na_xCo_2O_4$ (*74*). The following subsections discuss three spin-enabled mechanisms. Note that the Rashba effect and topological states add new components to the matrix of conventional charge-based thermoelectricity, whereas the spin Seebeck effect (SSE) is conceptually distinct.

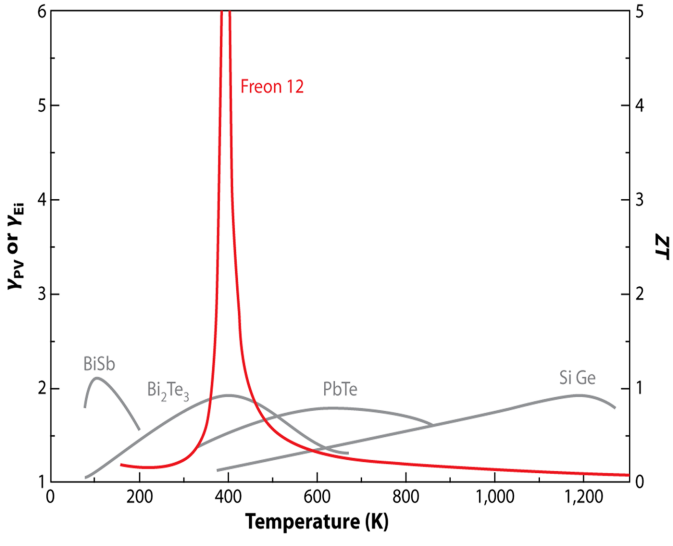

Fig. 4. The analogy between TE energy conversion and gas-cycle engines. A comparison between the ratio γ_{Ei} of Freon-12 and the ZT of several n-type TE materials as a function of temperature. [Figure adapted from (*9*)]

Rashba effect

The Rashba effect splits electron bands by the spin-orbit coupling (SOC) in crystals that lack an inversion center. The Rashba effect induces a sharp electronic DOS feature that results in an E_F much lower than the spin-degenerate case and also a more 2D-like Fermi surface (e.g., ring or elliptic torus). The sharp DOS feature near the E_F leads to an enhanced $|\alpha|$, resembling the quantum size effect. The Rashba effect is a key ingredient of many exotic spin-orbitronic phenomena such as the spin Hall effect, topological insulators

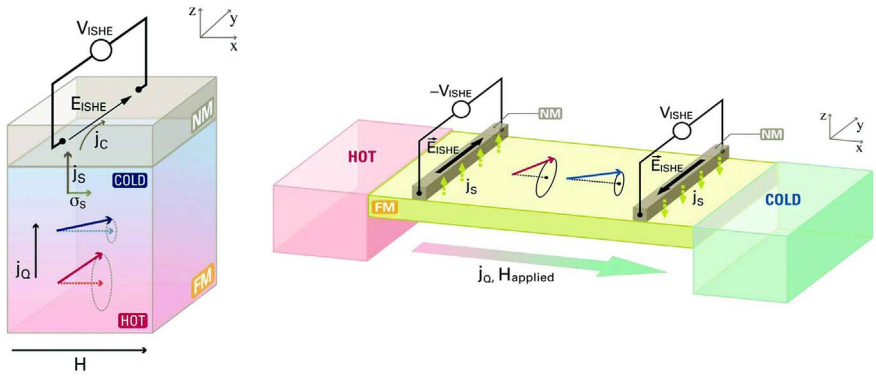

Fig. 5. Longitudinal and transverse spin Seebeck effect. (**Left**) Schematic diagram of the longitudinal spin Seebeck effect. The magnetization gradient in the ferromagnet (FM) transfers a pure spin current into the normal metal (NM, e.g., Pt). The inverse spin Hall effect V_{ISHE} of NM converts the pure spin current into a measurable transverse voltage drop, V_{ISHE}. (**Right**) Schematic diagram of nonlocal thermal spin injection from a magnon system, i.e., the transverse spin Seebeck effect. The heat flow in the FM leads to a longitudinal magnetization in the same direction; the resulting diffusive spin current perpendicular to the heat flow is detected as a V_{ISHE} in the NM. The j_C, j_S, j_Q, S, H ($H_{applied}$) are the charge flux, spin flux, heat flux, spin-indexed electrical conductivity, and the externally applied magnetic field, respectively. [Figure adapted from (*86*)]

(TIs), chiral magnonics, and spin interference (*75*). One signature of the Rashba effect is that the resulting band extrema are located off the high-symmetry directions in a Brillouin zone. BiTeX (X = I, Br, or Cl) is a good example of a Rashba TE material (*76*, and the references therein). Interestingly, the internal electric field induced by the Rashba effect might facilitate anharmonicity (*77*).

Topological states

Unlike the classical order of matter described by local symmetry and long-range correlation in the Landau symmetry-breaking theory, topological order arises from long-range entanglement of quantum states. In particular, TIs are the materials with a bulk band gap and topologically protected conducting edge (surface) states (*78*). To be a TI, a material needs to satisfy several criteria: (i) the presence of large SOC, (ii) an odd number of band inversions between the conduction and valence band, and (iii) a sign change of the symmetry of molecular orbitals (*79*). As heavy elements yield a large SOC effect and a low κ_L, both TIs and TE materials favor heavy elements and a bulk band gap. This is why many benchmark TE materials such as BiSb, Bi_2Te_3, and Bi_2Se_3 turned out to be TIs (*80*).

The edge states of TIs are topologically protected from back scattering and immune to defects unless the defects break the time-reversal symmetry. In addition, the Dirac bands render a large carrier mobility. These traits have attracted theoretical interest from the standpoint of thermoelectrics. Xu *et al.* discussed the strongly energy-dependent lifetime of edge states in TIs, the anomalous Seebeck coefficient, and the size dependence of *ZT* values (*81*). Zahid *et al.* studied the TE properties of Bi_2Te_3 atomic quintuple thin films (*82*). Liang *et al.* reported a high n-type TE performance in few–quintuple layer–thick Bi_2Te_3 when the system crossed from a topologically trivial regime to a topologically nontrivial regime (*83*). The recent work of Wei *et al.* revealed that the alternating stack structure of topologically nontrivial quantum spin Hall layers $[(RhBi_4)_3I]^{2+}$ and topologically trivial insulator layers $[Bi_2I_8]^{2-}$ in the weak TI $Bi_{14}Rh_3I_9$ yielded a minimum κ_L (*84*).

Spin Seebeck effect

The SSE is conceptually distinct from the conventional charge-based Seebeck effect (CSE). Especially, one should not confuse the SSE and the spin-dependent Seebeck effect: The spin-dependent Seebeck effect is no more than a spin-polarized CSE, whereas the SSE refers to the transverse spin voltage related to the nonequilibrium spin pumping driven by a longitudinal temperature difference and the inhomogeneous fluctuations between conduction electrons and magnons (Fig. 5). Boona *et al.* examined the emerging field of spin caloritronics, including the implications of SSE and magnon-electron drag effect in solid-state thermal-to-electrical energy conversions (*85*, *86*).

Despite its infancy and a generally weak intensity, the SSE has some advantages over the CSE in energy conversion. First, the flow geometry of SSE is reminiscent of the Nernst-Ettingshausen effect; the temperature gradient and the resulting electric field are spatially decoupled (compare Fig. 5). Increasing the power output of a spin Seebeck magneto-caloritronic (SSMC) device only requires increasing the physical size of the material, either p type or n type. By contrast, a charge-based TE device needs to connect more p-type and n-type legs thermally in parallel and electrically in series to increase the power output. Second, a SSMC device is optimized through separately optimizing the thermal and magnetic properties of the spin source material and the electrical properties of the spin sink material. By contrast, optimizing a charge-based TE device requires the optimization of (ρ, α, and κ) in their totality for both the p leg and the n leg. Notably, a giant SSE at cryogenic temperatures was reported in nonmagnetic InSb and attributed to the strong phonon-drag and SOC effect (*87*), which promises potential applications in low-temperature power generation, cooling, and sensing. Currently, there are only a few practical charge-based TE materials at cryogenic temperatures (*88*, *89*).

Other notable mechanisms

The optimal carrier concentration of a TE material generally increases with increasing temperature, but the doping level is often fixed in practice. Pei *et al.* utilized the temperature-dependent solubility of Ag in PbTe to self-tune the carrier concentration of PbTe-Ag_2Te composites over a wide temperature range (*90*). Zhao *et al.* used the magnetic transition of $BaFe_{12}O_{19}$ nanoparticles as an "electron repository" to suppress the detrimental bipolar effect and maintain high *ZT* values in the intrinsic excitation region of (Ba,In)-filled $CoSb_3$ (*91*). A multilocalization transport scenario was proposed for In-filled $CoSb_3$ (*92*). In strongly correlated systems, the many-body renormalizations, along with phonon mediation, give rise to peculiar TE responses, such as the giant low-temperature Seebeck coefficient of $FeSb_2$ (*93*). Sun *et al.* identified a new mechanism of enhancing the Seebeck coefficient via strongly temperature-dependent mobility (*94*). Yan *et al.* temporally modulated the temperature of the heat source and achieved a substantial enhancement of device efficiency (*95*). Norouzzadeh *et al.* examined the emerging role of valley degree of freedom in thermoelectrics in terms of band degeneracy and intervalley scattering (*96*).

Promising materials

Mechanisms are embodied in the material properties and thus the materials. To date, degenerate semiconductors remain the cornerstone of high-performance TE materials. In line with attaining a high *B* factor (Eq. 3), a set of material chemistry criteria has been developed to identify promising TE materials: (i) A high-symmetry crystal structure elicits high band degeneracy, which enhances the DOS at Fermi level without substantially degrading the charge-carrier mobility. (ii) A small electronegativity difference among the constituent elements yields covalent chemical bonding, which ensures a high charge-carrier mobility by suppressing localization and optical phonon scattering of charge carriers. (iii) A large complex unit cell with heavy atoms and strong anharmonicity renders a low intrinsic-lattice thermal conductivity. Strong spin-orbital coupling effect of heavy elements is desired for the Rashba effect and topological states.

The TE materials mentioned in preceding sections are in line with these criteria. Below we briefly review a number of promising TE materials, among which SnSe and oxides are, to some degree, the outliers of these criteria. Because of page limitations, the reader is referred to two

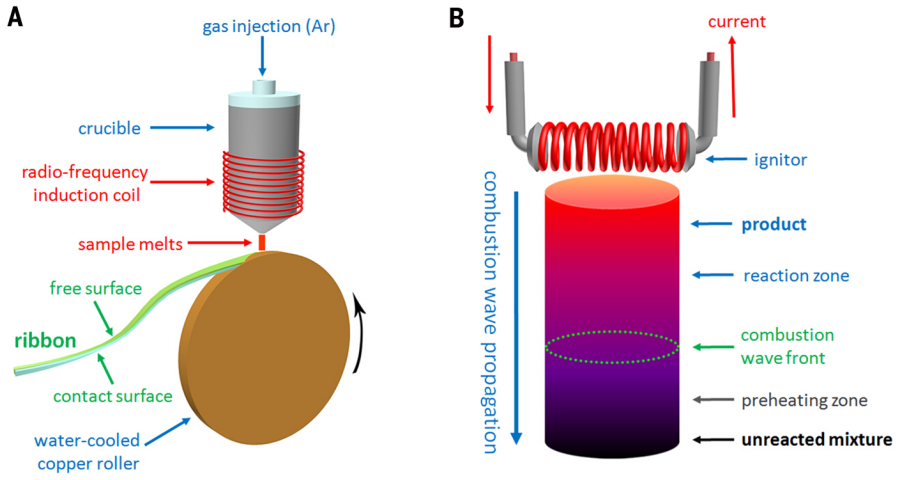

Fig. 6. Nonequilibrium material-synthesis recipes. Schematic diagram of (**A**) melt spinning (MS) and (**B**) self-propagation high-temperature synthesis (SHS). In a SHS process, the combustion wavefront is reminiscent of zone melting growth but at a much faster propagation rate.

recent reviews (*21*, *24*), and the references therein, for further information on lead and lead-free chalcogenides, clathrates, silicides, Zintl phases, half-Heusler MgAgSb, and BiCuSeO compounds.

SnSe

SnSe is a fascinating material characterized by strong anharmonicity and low κ_L (*97*); both traits are somewhat surprising in this seemingly simple binary compound that contains no heavy elements (e.g., Pb, Bi, Sb, or Te). In addition, SnSe adopts a low-symmetric crystal lattice; the space group below and above the displacive phase transition near 800 K are *Pnma* (#62) to *Cmcm* (#63), respectively. Li *et al.* used inelastic neutron scattering in conjunction with density functional theory calculations to ascribe the strong anharmonicity to the long-range resonant p-bond network of Se coupled to stereochemically active 5s orbitals of Sn (*98*). Despite a distinct crystal structure, SnSe is reminiscent of PbTe in terms of strong anharmonicity and the ferroelectric instability (*99*). In addition to the high p-type performance reported in Na-doped SnSe single crystals (*100*, *101*), a high n-type performance was attained in Bi-doped SnSe single crystals (*102*). There are some interesting questions that remain to be answered, e.g., what is the ground state of SnSe, the impact of native and extrinsic defects on the electrical transport and anharmonicity, and the performance improvement of polycrystalline SnSe materials?

Oxides

Oxides were considered poor TE materials because (i) the large electronegativity difference among the constituent elements leads to strong localization and charge-carrier scattering by optical phonons and, therefore, low μ and (ii) the large bonding energy and small mass of oxygen lead to a high velocity of sound and, therefore, high κ_L. Hence, the TE studies of Na_xCoO_2, ZnO, and Ruddlesden-Popper homologous series $A_{m+1}B_mO_{3m+1}$ are ground breaking and enlightening (*103*, *104*). Oxide TE materials are known for their availability, tunability, and thermal stability. The high operation temperature (>900 K) ensures a high Carnot efficiency in Eq. 1 that compensates for their moderate *ZT* values. The TE study of complex structured oxides is often in line with the phonon glass–electron crystal (PGEC) paradigm (*105*): A complex crystal structure can be regarded as formed by various building modules, each functioning as a phonon glass or an electron crystal. Thus, the electrical and thermal transport can be optimized separately in the corresponding building module.

Half-Heusler compounds

Like oxides, half-Heusler (HH) compounds also work in the high-temperature regime. HH compounds adopt a general formula of XYZ (X = transition metal, noble metal or rare-earth element; Y = transition metal or noble metal; and Z = main group element) and a face-centered crystal lattice. HH compounds are known for their mechanical robustness and thermal stability. Although they are traditionally described as intermetallics, it is instructive to understand the band structure and defect chemistry of HH compounds in the framework of Zintl-Klemm chemistry (*106*). One long-standing issue of HH compounds is a lack of balance between n-type and p-type performance: Higher performance p-type materials are needed. Fu *et al.* found heavy Hf-doping led to a *ZT* ~ 1.5 at 1200 K in heavy-band p-type FeNbSb with excellent mechanical strength and thermal stability (*107*). In Ti-doped p-type $FeV_{0.6}Nb_{0.4}Sb$, low deformation energy and low alloy scattering were utilized to mitigate the band effective masses that were otherwise too high (*108*).

Caged and open-framework structured materials

For decades, $CoSb_3$ skutterudite has been a benchmark mid-temperature TE material owing to its cagey structure for guest-atom filling. The filling-fraction limit is a major limitation on the material performance. Tang *et al.* devised a "solubility design" for Ce-filled $CoSb_3$ based on a deeper understanding of the ternary phase diagram, and the results provide new insights into the doping and filling of other higher multinary TE materials (*109*). Cu_2Se is open-framework structured and a mixed electronic-ionic conductor above ~400 K, and the Cu diffusion channels host multiscale disorder forms that render a phonon-liquid-like behavior (*110*, *111*). Note that the electromigration of Cu^+ ions under a temperature gradient will deplete the Cu^+ ions. Incorporating a small amount of In into the Cu_2Se lattice helps localize the Cu^+ ions, leading to a record high ZT_m ~ 1.5 over a broad temperature range and a maximum *ZT* value ~ 2.6 at 850 K in Cu_2Se-$CuInSe_2$ nanocomposites (*112*). In the layered-structure metal chalcogenides, the semiconducting gap and the van der Waals gap invite doping and intercalations, respectively (*113*–*115*). The synergy of Br-doping, Cu-intercalation, and nanoinclusions led to a *ZT* ~ 1.1 at 723 K in $In_4Se_{2.5}$ (*116*).

Other interesting materials

Despite moderate *ZT* values, some materials are promising in the long run as they are made of earth-abundant elements, exhibiting low intrinsic κ_L and/or having a large phase space for optimization. For example, the diamond-like compounds comprise a large number of higher multinary compounds in which the constituent elements are tetrahedrally coordinated in a cubic zinc blende or a noncubic chalcopyrite structure. They tend to have low intrinsic κ_L due to distorted tetrahedra and good mid-temperature TE performance upon band convergence (*21*, *45*). Tetrahedrites are another example. In $Cu_{12}Sb_4S_{13}$ tetrahedrite, Cu atoms occupy two distinct crystallographic sites at a 50:50 ratio (*117*). The crystal structure of $Cu_{12}Sb_4S_{13}$ can be viewed as a PGEC formed by (i) a cavity polyhedral formed by CuS_3 and SbS_3 groups that govern the thermal transport and (ii) the framework of CuS_4 groups that governs the electrical transport. Co-doping $Cu_{12}Sb_4S_{13}$ with Ni and Zn has led to a *ZT* ~ 1 (*118*). The organic TE materials, especially the composites based on conducting polymers poly-3,4-ethylenedioxythiophene (PEDOT) and polyaniline (PANI) (*119*, *120*), are paving a way toward cheap, flexible, printable, and stretchable TE modules.

Advanced synthesis and processing techniques

Developing next-generation TE materials must progress hand-in-hand with developing advanced material synthesis and processing techniques. High TE performance often requires delicate multiscale microstructures that traditional growth-from-the-melt or powder metallurgy recipes generally fall short of being able to prepare. The nonequilibrium recipes such as ball milling (BM), melt spinning (MS), and self-sustaining heating synthesis (SHS) hold promise as they can reach a much broader phase space. The Ren group at Boston College conducted high-energy ball-milling processing on a

wide range of TE materials; the resulting grain-size refinement and rich nanostructures led to performance enhancement (*121*). The Tang group at Wuhan University of Technology pioneered the MS (*122*, *123*) and SHS techniques [*124* (videos and supplementary materials), *125*] in making high-performance TE materials. Both the MS and SHS techniques (Fig. 6) are nonequilibrium recipes that can yield rich multiscale microstructures in single-phased ternary and even quaternary TE materials. The efficacy of these nonequilibrium recipes is restricted by the thermal stability of the as-formed microstructures.

The spark plasma–sintering (SPS) technique (*126*), i.e., field-assisted–sintering technique or pulsed–electric current sintering, is widely used in TE materials research. The SPS technique is a physical densification tool in general and a chemical reaction tool on occasion. Although the energy and time efficacy of the SPS process has proved to be outstanding, the sintering process is not yet fully understood on the microscopic level. For example, the presence of sparks and plasmas in the sintering process is questioned (*127*). Filling this gap of knowledge may lead to newer designs of sintering techniques. An emerging direction is the synergy of additive manufacture (3D printing) and machine learning, which may facilitate high-throughput materials screening and exploration of the ternary and quaternary phase space.

Perspective remarks

TE materials research is an application-driven fundamental research field bridging the disciplines of physics, chemistry, materials science, and mechanical engineering. High material performance builds on a delicate concert of hierarchical trade-offs, e.g., structural order and disorder, phase stability and instability, band convergence and splitting, effective mass and mobility, bond covalency, and ionicity. Although the TE materials research is application driven, it is the rich fundamental physics, chemistry, and materials science that actually drives the research. Today, emerging concepts such as topological states, the Rashba effect, the spin Seebeck effect, resonant levels, resonant bonding, and anharmonicity are keeping the field of TE materials research at the cutting edge of science.

After 60 years of fruitful work, the maximum *ZT* values have doubled, and, some might argue, essentially tripled. It may not sound that impressive, but in our opinion it is, given that a four-fold increase would have changed the renewable energy landscape. Thermoelectrics has specific technical advantages in distributed power generation and active spot-size heat management. Given the ubiquity of heat, thermoelectrics has secured a position in our total-package solution to global energy needs and environmental crisis. In the years to come, we expect scientists will look for more outliers of the current material-selection criteria; develop more high-performance TE materials out of nontoxic and earth-abundant elements; shift attention from power generation to refrigeration, as cooling is less cost-sensitive than power generation; and conduct high-throughput calculations and experiments in higher multinary compounds. Cross-checking the high *ZT* values of emerging materials by international round-robin studies is also crucial (*128*). The outcome of these efforts will shape the future of thermoelectrics over the next 20 years or more and, in turn, reshape the renewable energy landscape.

REFERENCES AND NOTES

1. Lawrence Livermore National Laboratory (LLNL) and the U.S. Department of Energy, "Energy flow charts—2015: United States"; https://flowcharts.llnl.gov/commodities/energy.
2. G. S. Nolas, J. Sharp, H. J. Goldsmid, *Thermoelectrics–Basic Principles and New Materials Developments* (Springer, 2001).
3. T. M. Tritt, M. A. Subramanian, Thermoelectric materials, phenomena, and applications: A bird's eye view. *MRS Bull.* **31**, 188–198 (2006). doi: 10.1557/mrs2006.44
4. G. J. Snyder, E. S. Toberer, Complex thermoelectric materials. *Nat. Mater.* **7**, 105–114 (2008). doi: 10.1038/nmat2090; pmid: 18219332
5. M. S. Dresselhaus *et al*., in *Chemistry, Physics, and Materials Science of Thermoelectric Materials*, M. G. Kanatzidis, S. D. Mahanti, T. P. Hogan, Eds. (Springer, 2003), pp. 1–17.
6. T. M. Tritt, H. Böttner, L. Chen, Thermoelectrics: Direct solar thermal energy conversion. *MRS Bull.* **33**, 366–368 (2008). doi: 10.1557/mrs2008.73
7. D. M. Nguyen, H. Xu, Y. Zhang, B. Zhang, Active thermal cloak. *Appl. Phys. Lett.* **107**, 121901 (2015). doi: 10.1063/1.4930989
8. P. Pichanusakorn, P. Bandaru, Nanostructured thermoelectrics. *Mater. Sci. Eng. Rep.* **67**, 19–63 (2010). doi: 10.1016/j.mser.2009.10.001
9. A. Shakouri, Recent developments in semiconductor thermoelectric physics and materials. *Annu. Rev. Mater. Res.* **41**, 399–431 (2011). doi: 10.1146/annurev-matsci-062910-100445
10. T. M. Tritt, Thermoelectrics run hot and cold. *Science* **272**, 1276–1277 (1996). doi: 10.1126/science.272.5266.1276
11. B. C. Sales, D. Mandrus, R. K. Williams, Filled skutterudite antimonides: A new class of thermoelectric materials. *Science* **272**, 1325–1328 (1996). doi: 10.1126/science.272.5266.1325; pmid: 8662465
12. R. P. Chasmar, R. Stratton, The thermoelectric figure of merit and its relation to thermoelectric generators. *J. Electron. Control* **7**, 52–72 (1959). doi: 10.1080/00207215908937186
13. G. D. Mahan, Good thermoelectrics in *Solid State Physics* (Academic Press, 1998), vol. 1, pp. 81–157.
14. H. Wang, Y. Z. Pei, A. D. LaLonde, G. J. Snyder, in *Thermoelectric Nanomaterials*, K. Koumoto, T. Mori, Eds. (Springer Series in Materials Science, Springer, 2013), vol. 182, pp. 3–32.
15. G. J. Snyder, T. S. Ursell, Thermoelectric efficiency and compatibility. *Phys. Rev. Lett.* **91**, 148301 (2003). doi: 10.1103/PhysRevLett.91.148301; pmid: 14611561
16. C. Goupil, W. Seifert, K. Zabrocki, E. Muller, G. J. Snyder, Thermodynamics of thermoelectric phenomenon and applications. *Entropy (Basel)* **12**, 1481–1517 (2013).
17. P. M. Chaikin, in *Organic Superconductivity*, V. Z. Kresin, W. A. Little, Eds. (Springer, 1990), pp. 101–115.
18. V. Yu. Irkhin, Yu. P. Irkhin, *Electronic Structure, Correlated Effects and Physical Properties of d- and f-Metals and Their Compounds* (Cambridge International Science Publishing, 2007).
19. T. E. Humphrey, H. Linke, Reversible thermoelectric nanomaterials. *Phys. Rev. Lett.* **94**, 096601 (2005). doi: 10.1103/PhysRevLett.94.096601; pmid: 15783983
20. H. B. Callen, The application of Onsager's reciprocal relations to thermoelectric, thermomagnetic, and galvanomagnetic effects. *Phys. Rev.* **73**, 1349–1358 (1948). doi: 10.1103/PhysRev.73.1349
21. X. Shi, L. Chen, C. Uher, Recent advances in high-performance bulk thermoelectric materials. *Int. Mater. Rev.* **61**, 379–415 (2016). doi: 10.1080/09506608.2016.1183075
22. C. J. Vineis, A. Shakouri, A. Majumdar, M. G. Kanatzidis, Nanostructured thermoelectrics: Big efficiency gains from small features. *Adv. Mater.* **22**, 3970–3980 (2010). doi: 10.1002/adma.201000839; pmid: 20661949
23. J.-F. Li, W.-S. Liu, L.-D. Zhao, M. Zhou, High-performance nanostructured thermoelectic materials. *NPG Asia Mater.* **2**, 152–158 (2010). doi: 10.1038/asiamat.2010.138
24. G. Tan, L. D. Zhao, M. G. Kanatzidis, Rationally designing high-performance bulk thermoelectric materials. *Chem. Rev.* **116**, 12123–12149 (2016). doi: 10.1021/acs.chemrev.6b00255; pmid: 27580481
25. W. G. Zeier *et al*., Thinking like a chemist: Intuition in thermoelectric materials. *Angew. Chem. Int. Ed.* **55**, 6826–6841 (2016). doi: 10.1002/anie.201508381; pmid: 27111867
26. M. Zebarjadi, K. Esfarjani, M. S. Dresselhaus, Z. F. Ren, G. Chen, Perspectives on thermoelectrics: From fundamentals to device applications. *Energy Environ. Sci.* **5**, 5147–5162 (2012). doi: 10.1039/C1EE02497C
27. T. J. Zhu *et al*., Compromise and synergy in high-efficiency thermoelectric materials. *Adv. Mater.* **29**, 1605884 (2017). doi: 10.1002/adma.201605884
28. K. Behnia, H. Aubin, Nernst effect in metals and superconductors: A review of concepts and experiments. *Rep. Prog. Phys.* **79**, 046502 (2016). doi: 10.1088/0034-4885/79/4/046502; pmid: 27010481
29. E. S. Toberer, L. L. Baranowski, C. Dames, Advances in thermal conductivity. *Annu. Rev. Mater. Res.* **42**, 179–209 (2012). doi: 10.1146/annurev-matsci-070511-155040
30. Z. T. Tian, S. Lee, G. Chen, Comprehensive review of heat transfer in thermoelectric materials and devices. *Annu. Rev. Heat Transf.* **17**, 425–483 (2014). doi: 10.1615/AnnualRevHeatTransfer.2014006932
31. A. Mehdizadeh Dehkordi, M. Zebarjadi, J. He, T. M. Tritt, Thermoelectric power factor: Enhancement mechanisms and strategies for higher performance thermoelectric materials. *Mater. Sci. Eng. Rep.* **97**, 1–22 (2015). doi: 10.1016/j.mser.2015.08.001
32. J. Yang *et al*., On the tuning of electrical and thermal transport in thermoelectrics: An integrated theory-experiment perspective. *npg Comput. Mater.* **2**, 15015 (2016). doi: 10.1038/npjcompumats.2015.15
33. C. Jeong, R. Kim, M. Luisier, S. Datta, M. Lundstrom, On Landauer versus Boltzmann and full band versus effective mass evaluation of thermoelectric transport coefficients. *J. Appl. Phys.* **107**, 023707 (2010). doi: 10.1063/1.3291120
34. Q. Zhang *et al*., Thermoelectric devices for power generation: Recent progress and future challenges. *Adv. Eng. Mater.* **18**, 194–213 (2016). doi: 10.1002/adem.201500333
35. Z. Li, C. Xiao, H. Zhu, Y. Xie, Defect chemistry for thermoelectric materials. *J. Am. Chem. Soc.* **138**, 14810–14819 (2016). doi: 10.1021/jacs.6b08748; pmid: 27802035
36. T. Zhu, L. Hu, X. Zhao, J. He, New insights into intrinsic point defects in V_2VI_3 thermoelectric materials. *Adv. Sci.* **3**, 1600004 (2016). doi: 10.1002/advs.201600004; pmid: 27818905
37. J. P. Heremans, B. Wiendlocha, A. M. Chamoire, Resonant levels in bulk thermoelectric semiconductors. *Energy Environ. Sci.* **5**, 5510–5530 (2012). doi: 10.1039/C1EE02612G
38. J. P. Heremans *et al*., Enhancement of thermoelectric efficiency in PbTe by distortion of the electronic density of states. *Science* **321**, 554–557 (2008). doi: 10.1126/science.1159725; pmid: 18653890
39. Y. Pei, H. Wang, G. J. Snyder, Band engineering of thermoelectric materials. *Adv. Mater.* **24**, 6125–6135 (2012). doi: 10.1002/adma.201202919; pmid: 23074043
40. Y. Pei *et al*., Convergence of electronic bands for high performance bulk thermoelectrics. *Nature* **473**, 66–69 (2011). doi: 10.1038/nature09996; pmid: 21544143
41. Y. Pei *et al*., Stabilizing the optimal carrier concentration for high thermoelectric efficiency. *Adv. Mater.* **23**, 5674–5678 (2011). doi: 10.1002/adma.201103153; pmid: 22052689
42. Y. Pei, H. Wang, Z. M. Gibbs, A. D. LaLonde, G. J. Snyder, Thermopower enhancement in Pb1-xMnxTe alloys and its effect on thermoelectric efficiency. *NPG Asia Mater.* **4**, e28 (2012). doi: 10.1038/am.2012.52
43. Y. Tang *et al*., Convergence of multi-valley bands as the electronic origin of high thermoelectric performance in $CoSb_3$ skutterudites. *Nat. Mater.* **14**, 1223–1228 (2015). doi: 10.1038/nmat4430; pmid: 26436339
44. W. Liu *et al*., Convergence of conduction bands as a means of enhancing thermoelectric performance of *n*-type $Mg_2Si_{1-x}Sn_x$ solid solutions. *Phys. Rev. Lett.* **108**, 166601 (2012). doi: 10.1103/PhysRevLett.108.166601; pmid: 22680741
45. J. Zhang *et al*., High-performance pseudocubic thermoelectric materials from non-cubic chalcopyrite compounds. *Adv. Mater.* **26**, 3848–3853 (2014). doi: 10.1002/adma.201400058; pmid: 24692165
46. Y. Chen *et al*., Transport properties and valence band feature of high-performance $(GeTe)_{85}(AgSbTe_2)_{15}$ thermoelectric materials. *New J. Phys.* **16**, 013057 (2014). doi: 10.1088/1367-2630/16/1/013057
47. G. Tan *et al*., Codoping in SnTe: Enhancement of thermoelectric performance through synergy of resonance

levels and band convergence. *J. Am. Chem. Soc.* **137**, 5100–5112 (2015). doi: 10.1021/jacs.5b00837; pmid: 25856499
48. O. V. Yazyev, Y. P. Chen, Polycrystalline graphene and other two-dimensional materials. *Nat. Nanotechnol.* **9**, 755–767 (2014). doi: 10.1038/nnano.2014.166; pmid: 25152238
49. S. I. Kim *et al*., Dense dislocation arrays embedded in grain boundaries for high-performance bulk thermoelectrics. *Science* **348**, 109–114 (2015). doi: 10.1126/science.aaa4166; pmid: 25838382
50. K. Biswas *et al*., High-performance bulk thermoelectrics with all-scale hierarchical architectures. *Nature* **489**, 414–418 (2012). doi: 10.1038/nature11439; pmid: 22996556
51. W. Xie *et al*., Identifying the specific nanostructures responsible for the high thermoelectric performance of $(Bi,Sb)_2Te_3$ nanocomposites. *Nano Lett.* **10**, 3283–3289 (2010). doi: 10.1021/nl100804a; pmid: 20687520
52. K. Biswas *et al*., Strained endotaxial nanostructures with high thermoelectric figure of merit. *Nat. Chem.* **3**, 160–166 (2011). doi: 10.1038/nchem.955; pmid: 21258390
53. L. D. Zhao *et al*., High thermoelectric performance via hierarchical compositionally alloyed nanostructures. *J. Am. Chem. Soc.* **135**, 7364–7370 (2013). doi: 10.1021/ja403134b; pmid: 23647245
54. A. I. Hochbaum *et al*., Enhanced thermoelectric performance of rough silicon nanowires. *Nature* **451**, 163–167 (2008). doi: 10.1038/nature06381; pmid: 18185582
55. X. Ji *et al*., Nanoscale granular boundaries in polycrystalline $Pb_{0.75}Sn_{0.25}Te$: An innovative approach to enhance the thermoelectric figure of merit. *Phys. Status Solidi., A Appl. Mater. Sci.* **206**, 221–228 (2009). doi: 10.1002/pssa.200824335
56. A. Shakouri, J. E. Bowers, Heterostructure integrated thermionic coolers. *Appl. Phys. Lett.* **71**, 1234–1236 (1997). doi: 10.1063/1.119861
57. P. Puneet *et al*., Preferential scattering by interfacial charged defects for enhanced thermoelectric performance in few-layered *n*-type Bi_2Te_3. *Sci. Rep.* **3**, 3212 (2013). doi: 10.1038/srep03212; pmid: 24225424
58. B. Poudel *et al*., High-thermoelectric performance of nanostructured bismuth antimony telluride bulk alloys. *Science* **320**, 634–638 (2008). doi: 10.1126/science.1156446; pmid: 18356488
59. B. R. Nag, *Electron Transport in Compound Semiconductors* (Springer, 1980).
60. M. Zebarjadi *et al*., Power factor enhancement by modulation doping in bulk nanocomposites. *Nano Lett.* **11**, 2225–2230 (2011). doi: 10.1021/nl201206d; pmid: 21553899
61. M. Ibáñez *et al*., High-performance thermoelectric nanocomposites from nanocrystal building blocks. *Nat. Commun.* **7**, 10766 (2016). doi: 10.1038/ncomms10766; pmid: 26948987
62. M. Zebarjadi, B. Liao, K. Esfarjani, M. Dresselhaus, G. Chen, Enhancing the thermoelectric power factor by using invisible dopants. *Adv. Mater.* **25**, 1577–1582 (2013). doi: 10.1002/adma.201204802; pmid: 23325546
63. D. G. Cahill, S. K. Watson, R. O. Pohl, Lower limit to the thermal conductivity of disordered crystals. *Phys. Rev. B* **46**, 6131–6140 (1992). doi: 10.1103/PhysRevB.46.6131; pmid: 10002297
64. L. D. Hicks, M. S. Dresselhaus, Effect of quantum-well structures on the thermoelectric figure of merit. *Phys. Rev. B* **47**, 12727–12731 (1993). doi: 10.1103/PhysRevB.47.12727; pmid: 10005469
65. L. D. Hicks, M. S. Dresselhaus, Thermoelectric figure of merit of a one-dimensional conductor. *Phys. Rev. B* **47**, 16631–16634 (1993). doi: 10.1103/PhysRevB.47.16631; pmid: 10006109
66. C. B. Vining, The thermoelectric process. *Proc. MRS* **478**, 3–13 (1997). doi: 10.1557/PROC-478-3
67. H. Liu *et al*., Ultrahigh thermoelectric performance by electron and phonon critical scattering in $Cu_2Se_{1-x}I_x$. *Adv. Mater.* **25**, 6607–6612 (2013). doi: 10.1002/adma.201302660; pmid: 24018747
68. D. R. Brown *et al*., Phase transition enhanced thermoelectric figure-of-merit in copper chalcogenides. *APL Mater.* **1**, 052107 (2013). doi: 10.1063/1.4827595
69. D. T. Morelli, V. Jovovic, J. P. Heremans, Intrinsically minimal thermal conductivity in cubic I–V–VI_2 semiconductors. *Phys. Rev. Lett.* **101**, 035901 (2008). doi: 10.1103/PhysRevLett.101.035901; pmid: 18764265
70. G. A. Slack, The thermal conductivity of nonmetallic crystals. *Solid State Phys.* **34**, 1–71 (1979). doi: 10.1016/S0081-1947(08)60359-8
71. S. Lee *et al*., Resonant bonding leads to low lattice thermal conductivity. *Nat. Commun.* **5**, 3525 (2014). doi: 10.1038/ncomms4525; pmid: 24770354
72. T. Matsunaga *et al*., Phase-change materials: Vibrational softening upon crystallization and its impact on thermal properties. *Adv. Funct. Mater.* **21**, 2232–2239 (2011). doi: 10.1002/adfm.201002274
73. H. Jin *et al*., Phonon-induced diamagnetic force and its effect on the lattice thermal conductivity. *Nat. Mater.* **14**, 601–606 (2015). doi: 10.1038/nmat4247; pmid: 25799325
74. Y. Wang, N. S. Rogado, R. J. Cava, N. P. Ong, Spin entropy as the likely source of enhanced thermopower in $Na_xCo_2O_4$. *Nature* **423**, 425–428 (2003). doi: 10.1038/nature01639; pmid: 12761545
75. A. Manchon, H. C. Koo, J. Nitta, S. M. Frolov, R. A. Duine, New perspectives for Rashba spin-orbit coupling. *Nat. Mater.* **14**, 871–882 (2015). doi: 10.1038/nmat4360; pmid: 26288976
76. L. Wu *et al*., Enhanced thermoelectric performance in the Rashba semiconductor BiTeI through band gap engineering. *J. Phys. Condens. Matter* **28**, 085801 (2016). doi: 10.1088/0953-8984/28/8/085801; pmid: 26829207
77. L. H. Wu *et al*., Two-dimensional thermoelectrics with Rashba spin-split bands in bulk BiTeI. *Phys. Rev. B* **90**, 195210 (2014). doi: 10.1103/PhysRevB.90.195210
78. M. Z. Hasan, C. L. Kane, Colloquium: Topological insulators. *Rev. Mod. Phys.* **82**, 3045–3067 (2010). doi: 10.1103/RevModPhys.82.3045
79. L. Müchler *et al*., Topological insulators from a chemist's perspective. *Angew. Chem. Int.* **51**, 7221–7225 (2012). doi: 10.1002/anie.201202480; pmid: 22684869
80. H. J. Zhang *et al*., Topological insulators in Bi_2Se_3, Bi_2Te_3, and Sb_2Te_3 with a single Dirac cone on the surface. *Nat. Phys.* **5**, 438–442 (2009). doi: 10.1038/nphys1270
81. Y. Xu, Z. Gan, S.-C. Zhang, Enhanced thermoelectric performance and anomalous Seebeck effects in topological insulators. *Phys. Rev. Lett.* **112**, 226801 (2014). doi: 10.1103/PhysRevLett.112.226801; pmid: 24949782
82. F. Zahid, R. Lake, Thermoelectric properties of Bi_2Te_3 atomic quintuple thin films. *Appl. Phys. Lett.* **97**, 212102 (2010). doi: 10.1063/1.3518078
83. J. Liang, L. Cheng, J. Zhang, H. Liu, Z. Zhang, Maximizing the thermoelectric performance of topological insulator Bi_2Te_3 films in the few-quintuple layer regime. *Nanoscale* **8**, 8855–8862 (2016). doi: 10.1039/C6NR00724D; pmid: 27071548
84. P. Wei *et al*., Minimum thermal conductivity in weak topological insulators with Bimuth-based stace structure. *Adv. Funct. Mater.* **26**, 5360–5367 (2016). doi: 10.1002/adfm.201600718
85. S. R. Boona, S. J. Watzman, J. P. Heremans, Research update: Utilizing magnetization dynamics in solid-state thermal energy conversion. *APL Mater.* **4**, 104502 (2016). doi: 10.1063/1.4955027
86. S. R. Boona, R. C. Myers, J. P. Heremans, Spin caloritronics. *Energy Environ. Sci.* **7**, 885–910 (2014). doi: 10.1039/c3ee43299h
87. C. M. Jaworski, R. C. Myers, E. Johnston-Halperin, J. P. Heremans, Giant spin Seebeck effect in a non-magnetic material. *Nature* **487**, 210–213 (2012). doi: 10.1038/nature11221; pmid: 22785317
88. J. P. Heremans, H. Y. Jin, Y. H. Zheng, S. J. Watzman, A. Prakash, "BiSb and spin-related thermoelectric phenomena," in *Tri-Technology Device Refrigeration (TTDR)*, R. I. Epstein, B. F. Andresen, M. P. Hehlen, J. P. Heremans, I. N. Rühlich, M. Sheik-Bahae, Eds. (Proceedings of SPIE, 98210I, Bellingham, WA, 2016), vol. 9821.
89. D. Y. Chung *et al*., $CsBi_4Te_6$: A high-performance thermoelectric material for low-temperature applications. *Science* **287**, 1024–1027 (2000). doi: 10.1126/science.287.5455.1024; pmid: 10669411
90. Y. Z. Pei, A. F. May, G. J. Snyder, Self-tuning the carrier concentration of PbTe/Ag_2Te composites with excess Ag for high thermoelectric performance. *Adv. Energy Mater.* **1**, 291–296 (2011). doi: 10.1002/aenm.201000072
91. W. Zhao *et al*., Magnetoelectric interaction and transport behaviours in magnetic nanocomposite thermoelectric materials. *Nat. Nanotechnol.* **12**, 55–60 (2017). doi: 10.1038/nnano.2016.182; pmid: 27723733
92. W. Zhao *et al*., Multi-localization transport behaviour in bulk thermoelectric materials. *Nat. Commun.* **6**, 6197 (2015). doi: 10.1038/ncomms7197; pmid: 25648419
93. J. M. Tomczak, K. Haule, T. Miyake, A. Georges, G. Kotliar, Thermopower of correlated semiconductors: Application to $FeAs_2$ and $FeSb_2$. *Phys. Rev. B* **82**, 085104 (2010). doi: 10.1103/PhysRevB.82.085104
94. P. Sun *et al*., Large Seebeck effect by charge-mobility engineering. *Nat. Commun.* **6**, 7475 (2015). doi: 10.1038/ncomms8475; pmid: 26108283
95. Y. Yan, J. A. Malen, Periodic heating amplifies the efficiency of thermoelectric energy conversion. *Energy Environ. Sci.* **6**, 1267–1273 (2013). doi: 10.1039/c3ee24158k
96. P. Norouzzadeh, D. Vashaee, Classification of valleytronics in thermoelectricity. *Sci. Rep.* **6**, 22724 (2016). doi: 10.1038/srep22724; pmid: 26972331
97. L. D. Zhao *et al*., Ultralow thermal conductivity and high thermoelectric figure of merit in SnSe crystals. *Nature* **508**, 373–377 (2014). doi: 10.1038/nature13184; pmid: 24740068
98. C. W. Li *et al*., Orbitally driven giant phonon anharmonicity in SnSe. *Nat. Phys.* **11**, 1063–1069 (2015). doi: 10.1038/nphys3492
99. Y. Zhang, X. Ke, P. R. C. Kent, J. Yang, C. Chen, Anomalous lattice dynamics near the ferroelectric instability in PbTe. *Phys. Rev. Lett.* **107**, 175503 (2011). doi: 10.1103/PhysRevLett.107.175503; pmid: 22107535
100. L. D. Zhao *et al*., Ultrahigh power factor and thermoelectric performance in hole-doped single-crystal SnSe. *Science* **351**, 141–144 (2016). doi: 10.1126/science.aad3749; pmid: 26612831
101. K. Peng *et al*., Broad temperature plateau for high *ZT*s in heavily doped p-type SnSe single crystals. *Energy Environ. Sci.* **9**, 454–460 (2016). doi: 10.1039/C5EE03366G
102. A. T. Duong *et al*., Achieving *ZT*=2.2 with Bi-doped *n*-type SnSe single crystals. *Nat. Commun.* **7**, 13713 (2016). doi: 10.1038/ncomms13713; pmid: 27941762
103. K. Koumoto, Y. F. Wang, R. Z. Zhang, A. Kosuga, R. Funahashi, Oxide thermoelectric materials: A nanostructuring approach. *Annu. Rev. Mater. Res.* **40**, 363–394 (2010). doi: 10.1146/annurev-matsci-070909-104521
104. J. He, Y. Liu, R. Funahashi, Oxide thermoelectrics: The challenges, progress and outlook. *J. Mater. Res.* **26**, 1762–1772 (2011). doi: 10.1557/jmr.2011.108
105. G. A. Slack, in *CRC Handbook of Thermoelectricity*, R. M. Rowe, Ed. (CRC Press, 1995), pp. 407–440.
106. W. G. Zeier *et al*., Engineering half-Heusler thermoelectric materials using Zintl chemistry. *Nat. Rev. Mater.* **1**, 16032 (2016). doi: 10.1038/natrevmats.2016.32
107. C. Fu *et al*., Realizing high figure of merit in heavy-band *p*-type half-Heusler thermoelectric materials. *Nat. Commun.* **6**, 8144 (2015). doi: 10.1038/ncomms9144; pmid: 26330371
108. C. Fu *et al*., High band degeneracy contributes to high thermoelectric performance in p-type half-Heusler compounds. *Adv. Energy Mater.* **4**, 1400600 (2014). doi: 10.1002/aenm.201400600
109. Y. Tang, R. Hanus, S.-W. Chen, G. J. Snyder, Solubility design leading to high figure of merit in low-cost Ce-$CoSb_3$ skutterudites. *Nat. Commun.* **6**, 7584 (2015). doi: 10.1038/ncomms8584; pmid: 26189943
110. H. Liu *et al*., Copper ion liquid-like thermoelectrics. *Nat. Mater.* **11**, 422–425 (2012). doi: 10.1038/nmat3273; pmid: 22406814
111. P. Lu *et al*., Multiformity and fluctuation of Cu ordering in Cu_2Se thermoelectric materials. *J. Mater. Chem. A Mater. Energy Sustain.* **3**, 6901–6908 (2015). doi: 10.1039/C4TA07100J
112. A. A. Olvera *et al*., Partial indium solubility induces chemical stability and colossal thermoelectric figure of merit in Cu_2Se. *Energy Environ. Sci.* **10**, 1668–1676 (2017). doi: 10.1039/C7EE01193H
113. E. Guilmeau, Y. Breard, A. Maignan, Transport and thermoelectric properties in copper intercalated TiS_2 chalcogenide. *Appl. Phys. Lett.* **99**, 052107 (2011). doi: 10.1063/1.3621834
114. R. T. Littleton IV, T. M. Tritt, J. W. Koils, D. R. Ketchum, Transition-metal pentatellurides as potential low-temperature thermoelectric refrigeration materials. *Phys. Rev. B* **60**, 13453–13457 (1999). doi: 10.1103/PhysRevB.60.13453
115. C. Wan *et al*., Flexible n-type thermoelectric materials by organic intercalation of layered transition metal dichalcogenide TiS_2. *Nat. Mater.* **14**, 622–627 (2015). doi: 10.1038/nmat4251; pmid: 25849369
116. Y. Luo *et al*., Enhancement of the thermoelectric performance of polycrystalline $In_4Se_{2.5}$ by copper intercalation and bromine substitution. *Adv. Energy Mater.* **4**, 1300599 (2014). doi: 10.1002/aenm.201300599
117. X. Lu *et al*., High performance thermoelectricity in earth-abundant compounds based on natural mineral tetrahedrites. *Adv. Energy Mater.* **3**, 342–348 (2013). doi: 10.1002/aenm.201200650

118. X. Lu, D. T. Morelli, Y. Xia, V. Ozolins, Increasing the thermoelectric figure of merit of tetrahedrites by co-doping with nickel and zinc. *Chem. Mater.* **27**, 408–413 (2015). doi: 10.1021/cm502570b
119. G. H. Kim, L. Shao, K. Zhang, K. P. Pipe, Engineered doping of organic semiconductors for enhanced thermoelectric efficiency. *Nat. Mater.* **12**, 719–723 (2013). doi: 10.1038/nmat3635; pmid: 23644522
120. Q. Yao, Q. Wang, L. M. Wang, L. D. Chen, Abnormally enhanced thermoelectric transport properties of SWNT/PANI hybrid films by strengthened PANI molecular ordering. *Energy Environ. Sci.* **7**, 3801–3807 (2014). doi: 10.1039/C4EE01905A
121. Y. Lan, A. J. Minnich, G. Chen, Z. Ren, Enhancement of thermoelectric figure-of-merit by a bulk nanostructuring approach. *Adv. Funct. Mater.* **20**, 357–376 (2010). doi: 10.1002/adfm.200901512
122. W. J. Xie, X. F. Tang, Y. G. Yan, Q. J. Zhang, T. M. Tritt, Unique nanostructures and enhanced thermoelectric performance of melt-spun BiSbTe alloys. *Appl. Phys. Lett.* **94**, 102111 (2009). doi: 10.1063/1.3097026
123. H. Li, X. F. Tang, Q. J. Zhang, C. Uher, Rapid preparation method of bulk nanostructured $Yb_{0.3}Co_4Sb_{12+y}$ compounds and their improved thermoelectric performance. *Appl. Phys. Lett.* **93**, 252109 (2008). doi: 10.1063/1.3054158
124. X. Su *et al*., Self-propagating high-temperature synthesis for compound thermoelectrics and new criterion for combustion processing. *Nat. Commun.* **5**, 4908 (2014). doi: 10.1038/ncomms5908; pmid: 25223333
125. X. F. Tang, X. L. Su, Q. J. Zhang, C. Uher, in *Materials Aspect of Thermoelectricity*, C. Uher, Ed. (CRC Press, 2016), pp. 541–582.
126. Z. A. Munir, U. Anselmi-Tamburini, M. Ohyanagi, The effect of electric field and pressure on the synthesis and consolidation of materials: A review of the spark plasma sintering. *J. Mater. Sci.* **41**, 763–777 (2006). doi: 10.1007/s10853-006-6555-2
127. Y. F. Liu, D. H. Liebenberg, Electromagnetic radio frequency heating in the pulsed electric current sintering (PECS) process. *MRS Commun.* **7**, 266–271 (2017). doi: 10.1557/mrc.2017.35
128. H. Wang *et al*., International round-robin study of the thermoelectric transport of an *n*-type half-Heusler compound from 300 K to 773 K. *J. Electron. Mater.* **44**, 4482–4491 (2015). doi: 10.1007/s11664-015-4006-z
129. K. F. Hsu *et al*., Cubic $AgPb_mSbTe_{2+m}$: Bulk thermoelectric materials with high figure of merit. *Science* **303**, 818–821 (2004). doi: 10.1126/science.1092963; pmid: 14764873
130. Y. Pei *et al*., Convergence of electronic bands for high performance bulk thermoelectrics. *Nature* **473**, 66–69 (2011). doi: 10.1038/nature09996; pmid: 21544143
131. T. Fu *et al*., Enhanced thermoelectric performance of PbTe bulk materials with figure of merit $zT > 2$ by multi-functional alloying. *J. Materiomics* **2**, 141–149 (2016). doi: 10.1016/j.jmat.2016.05.005
132. L. D. Zhao *et al*., High thermoelectric performance via hierarchical compositionally alloyed nanostructures. *J. Am. Chem. Soc.* **135**, 7364–7370 (2013). doi: 10.1021/ja403134b; pmid: 23647245
133. H. Wang, Y. Pei, A. D. LaLonde, G. J. Snyder, Weak electron-phonon coupling contributing to high thermoelectric performance in n-type PbSe. *Proc. Natl. Acad. Sci. U.S.A.* **109**, 9705–9709 (2012). doi: 10.1073/pnas.1111419109; pmid: 22615358
134. L. D. Zhao *et al*., High performance thermoelectrics from earth-abundant materials: Enhanced figure of merit in PbS by second phase nanostructures. *J. Am. Chem. Soc.* **133**, 20476–20487 (2011). doi: 10.1021/ja208658w; pmid: 22126301
135. H. Wang, E. Schechtel, Y. Z. Pei, G. J. Snyder, High thermoelectric efficiency of n-type PbS. *Adv. Energy Mater.* **3**, 488–495 (2013). doi: 10.1002/aenm.201200683
136. B. Zhong *et al*., High superionic conduction arising from aligned large lamellae and large figure of merit in bulk $Cu_{1.94}Al_{0.02}Se$. *Appl. Phys. Lett.* **105**, 123902 (2014). doi: 10.1063/1.4896520
137. Z. H. Ge *et al*., Synthesis and transport property of $Cu_{1.8}S$ as a promising thermoelectric compound. *Chem. Commun. (Camb.)* **47**, 12697–12699 (2011). doi: 10.1039/c1cc16368j; pmid: 22048217
138. Y. He *et al*., High thermoelectric performance in non-toxic earth-abundant copper sulfide. *Adv. Mater.* **26**, 3974–3978 (2014). doi: 10.1002/adma.201400515; pmid: 24677586
139. J. Zhang *et al*., Discovery of high-performance low-cost n-type Mg_3Sb_2-based thermoelectric materials with multi-valley conduction bands. *Nat. Commun.* **8**, 13901 (2017). doi: 10.1038/ncomms13901; pmid: 28059069
140. G. Joshi *et al*., Enhanced thermoelectric figure-of-merit in nanostructured p-type silicon germanium bulk alloys. *Nano Lett.* **8**, 4670–4674 (2008). doi: 10.1021/nl8026795; pmid: 19367858
141. B. Yu *et al*., Enhancement of thermoelectric properties by modulation-doping in silicon germanium alloy nanocomposites. *Nano Lett.* **12**, 2077–2082 (2012). doi: 10.1021/nl3003045; pmid: 22435933
142. S. Bathula *et al*., Enhanced thermoelectric figure-of-merit in spark plasma sintered nanostructured n-type SiGe alloys. *Appl. Phys. Lett.* **101**, 213902 (2012). doi: 10.1063/1.4768297
143. L. D. Zhao *et al*., $Bi_{1-x}Sr_xCuSeO$ oxyselenides as promising thermoelectric materials. *Appl. Phys. Lett.* **97**, 092118 (2010). doi: 10.1063/1.3485050
144. L. D. Zhao *et al*., BiCuSeO oxyselenides new promising thermoelectric materials. *Energy Environ. Sci.* **7**, 2900–2924 (2014). doi: 10.1039/C4EE00997E
145. T. Plirdpring *et al*., Chalcopyrite $CuGaTe_2$: A high-efficiency bulk thermoelectric material. *Adv. Mater.* **24**, 3622–3626 (2012). doi: 10.1002/adma.201200732; pmid: 22689017
146. Y. Luo *et al*., Progressive regulation of electrical and thermal transport properties to high-performance $CuInTe_2$ thermoelectric materials. *Adv. Energy Mater.* **6**, 1600007 (2016). doi: 10.1002/aenm.201600007
147. X. Shi *et al*., Multiple-filled skutterudites: High thermoelectric figure of merit through separately optimizing electrical and thermal transports. *J. Am. Chem. Soc.* **133**, 7837–7846 (2011). doi: 10.1021/ja111199y; pmid: 21524125
148. G. Rogl *et al*., n-Type skutterudites $(R,Ba,Yb)_yCo_4Sb_{12}$ (R= Sr, La, Mm, DD, SrMm, SrDD) approaching ZT ≈ 2.0. *Acta Mater.* **63**, 30–43 (2014). doi: 10.1016/j.actamat.2013.09.039
149. S. Yamaguchi, T. Matsumoto, J. Yamazaki, N. Kaiwa, A. Yamamoto, Thermoelectric properties and figure of merit of a Te-doped InSb bulk single crystal. *Appl. Phys. Lett.* **87**, 201902 (2005). doi: 10.1063/1.2130390
150. Y. Cheng *et al*., New insight into InSb-based thermoelectric materials from a divorced eutectic design to a remarkably high thermoelectric performance. *J. Mater. Chem. A Mater. Energy Sustain.* **5**, 5163–5170 (2017). doi: 10.1039/C6TA10827J
151. G. Joshi *et al*., Enhancement in thermoelectric figure-of-merit of an n-type half-Heusler compound by the nanocomposite approach. *Adv. Energy Mater.* **1**, 643–647 (2011). doi: 10.1002/aenm.201100126
152. X. Yan *et al*., Thermoelectric property study of nanostructured p-type half-Heuslers (Hf, Zr,Ti)$CoSb_{0.8}Sn_{0.2}$. *Adv. Energy Mater.* **3**, 1195–1200 (2013). doi: 10.1002/aenm.201200973

ACKNOWLEDGMENTS

The authors thank P. C. Wei for enlightening discussions and Y. F. Liu, D. W. Yang, D. H. Liebenberg, M. McKenna, F. C. Meng, and M. H. Zhou for their assistance in preparing the figures and the manuscript. This work is supported by NSF Division of Materials Research (DMR) award 1307740.

10.1126/science.aak9997

Science

Advances in thermoelectric materials research: Looking back and moving forward

Jian He and Terry M. Tritt

Science **357** (6358), eaak9997.
DOI: 10.1126/science.aak9997

Strategies for efficient thermoelectrics

Thermoelectric materials convert heat into electricity and can provide solid-state cooling for spot-sized refrigeration. One important barrier for adopting these materials beyond niche applications is their low efficiency. He and Tritt review the mechanisms and strategies for improving thermoelectric efficiency. They discuss how to report material performance and highlight the most promising materials. With new materials and strategies for performance enhancement, thermoelectrics are poised to alter the renewable energy landscape.

Science, this issue p. eaak9997